

PAPER • **OPEN ACCESS**

Neutron yield scaling law in laser-cluster fusion experiments



To cite this article: Junho Won *et al* 2023 *Nucl. Fusion* **63** 066031

View the [article online](#) for updates and enhancements.

You may also like

- [Neutron yield as a measure of achievement nuclear fusion using a mixture of deuterium and tritium isotopes](#)
Ahmed Youssef, Rania Anwar, Ibrahim I Bashter et al.
- [Efficient generation of fast neutrons by magnetized deuterons in an optimized deuterium gas-puff z-pinch](#)
D Klir, A V Shishlov, V A Kokshenev et al.
- [Efficient generation of fusion neutrons from cryogenically cooled heteronuclear clusters irradiated by intense femtosecond lasers](#)
Hui Zhang, Haiyang Lu, Song Li et al.

Neutron yield scaling law in laser-cluster fusion experiments

Junho Won^{1,2} , Jaehyun Song^{1,2}, Seongmin Lee^{1,2}, Chiwan Song^{1,2} and Woosuk Bang^{1,2,*} 

¹ Department of Physics and Photon Science, GIST, Gwangju 61005, Korea, Republic Of

² Center for Relativistic Laser Science, Institute for Basic Science, Gwangju 61005, Korea, Republic Of

E-mail: wbang@gist.ac.kr

Received 12 August 2022, revised 20 March 2023

Accepted for publication 18 April 2023

Published 9 May 2023



Abstract

We present a scaling law ($Y \sim E^\beta$) of fusion neutron yields (Y) for laser pulse energy (E) in laser-cluster fusion experiments. We compare the available neutron yield data from previous deuterium cluster fusion experiments with those calculated using the cylindrical fusion plasma model. The calculated neutron yields are shown as functions of the incident laser pulse energy, average number density, and ion temperature. Although the deuterium–deuterium fusion reactivity is known to increase rapidly with ion temperature, the neutron yield shows a modest increase above ~ 10 keV for a given laser pulse energy. We find the scaling exponent β approaching 1.0 as the ion temperature increases from 1 keV to 100 keV. We explain the observed temperature dependence of β by examining the temperature dependence of the beam–beam and beam–target fusion neutron yields separately. Our scaling law differs from previously reported scaling laws from individual experiments, but it shows an excellent agreement with the scaling law determined by the maximum neutron yields of individual experiments.

Supplementary material for this article is available [online](#)

Keywords: laser fusion, laser-cluster fusion, nuclear fusion, fusion yield

(Some figures may appear in colour only in the online journal)

1. Introduction

Nuclear fusion is a highly nonlinear phenomenon [1], whose reaction rate depends heavily on several physical parameters such as the plasma density, volume, temperature, and fusion cross sections. When two energetic deuterium ions collide with each other, sometimes quantum tunneling [1] happens and Deuterium–Deuterium (DD) fusion reactions can occur.

To estimate the rate of nuclear fusion reactions, physicists have often described the probability of fusion reactions using cross sections [2]. The fusion cross section depends very strongly on the kinetic energy of the interacting particles [2], and this results in a rapid increase in the fusion cross section with the plasma temperature in the 1 keV to 100 keV range.

In laser-cluster fusion experiments [3, 4], an intense laser pulse irradiates deuterium fuels called deuterium clusters and produces energetic deuterium ions with typical temperatures exceeding multi-keV [5]. Laser-cluster fusion experiments have been studied for basic science, such as measuring fusion cross sections [6–8] as well as for practical applications, such as neutron sources in radiography or in time-resolved spectroscopy [9]. Neutron sources from laser-cluster fusion experiments do not require a large-scale laser facility and may

* Author to whom any correspondence should be addressed.



Original content from this work may be used under the terms of the [Creative Commons Attribution 4.0 licence](#). Any further distribution of this work must maintain attribution to the author(s) and the title of the work, journal citation and DOI.

offer adequate flux for materials studies at a high repetition rate [9, 10].

To maximize the fusion neutron yield under given experimental conditions, it is necessary to optimize the relevant physical parameters such as the laser pulse energy, pulse duration, beam size, gas jet backing pressure, temperature, and nozzle diameter. Finding the key parameters and optimizing them are, however, quite challenging because the laser-cluster parameters are very much correlated [11, 12], and many phenomena caused by the laser-cluster interaction occur nonlinearly [11–15]. So far, 10^5 – 10^6 fusion neutrons per joule of incident laser energy have been demonstrated experimentally [3, 10, 12, 16].

The cylindrical fusion plasma model is a simple but powerful model for calculating fusion yields in laser-cluster fusion experiments [17]. In the cylindrical fusion plasma model, fusion neutrons are produced from a symmetrically expanding deuterium fusion plasma [17]. The cylindrical fusion plasma is often approximated as homogeneous, which is a valid assumption considering the fast (several tens of fs) cluster ionization and explosion time scales compared with the much longer disassembly time (\sim ns) of the fusion plasma. (See supplementary figure S2 for more details.) In [11], the authors attempted to find the optimum laser-cluster parameters for the maximum neutron yield using the cylindrical fusion plasma model. In [17], the authors calculated the fusion yield as a function of time along with the corresponding disassembly time of the fusion plasma.

Laser-cluster fusion experiments have also been studied using Molecular Dynamics (MD) simulations, which provided information for laser-cluster dynamics such as inner and outer ionization [18], x-ray emission [19], electron-ion energy distribution [20–22], and conversion efficiency from laser energy to ion kinetic energy [20, 22]. Some studies have calculated neutron yields using the MD simulation as well. In [21, 22], the authors investigated the optimum conditions for deuterium cluster size and incident laser intensity. In [20], the effects of deuterium cluster size and inter-cluster distance on neutron yields were reported. Although these studies were mostly limited to a 1-dimensional (1D) slab model owing to insufficient computation power, MD simulations provided some valuable information regarding the plasma properties in laser-cluster fusion experiments [20–22].

As laser-cluster fusion experiments have often been performed in small-scale laser facilities, many earlier studies have attempted to provide neutron yield scaling laws based on their experimental findings. The scaling law of neutron yield for laser energy ($Y = \alpha E^\beta$) has been regarded as an essential tool for estimating the expected fusion neutron yield at a given laser energy. Identifying the correct scaling law is very important because it can predict the fusion yield for a laser energy region that has been previously unexplored. Regrettably, many earlier studies have presented different scaling laws based on their own investigations. For example, one experimental study reported a scaling law of $Y \sim E^{2.2}$ in the laser energy range extending from 0.025 J to 0.12 J [12]. In [23], the authors reported a scaling law of $Y \sim E^{1.6}$ for laser energy varying from 0.1 J to 5.5 J. In [23, 24], a scaling law

of $Y \sim E^{2.15-2.29}$ was found for the energy range extending from 0.1 J to 10 J. In a more recent study [25], a scaling exponent of 1.65 was obtained in the wide energy range from 1 mJ to 1.5 mJ. This scaling law was derived from extensive laser-induced fusion experiments including inertial confinement fusion experiments and laser-cluster fusion experiments. Interestingly, theoretical studies have also presented several different scaling laws corresponding to scaling exponents β varying from 1.2 to 2.0 [11, 12, 26, 27].

In this study, we aim to provide the correct scaling law for neutron yields from laser-cluster fusion experiments. We accomplish this by examining the available experimental data and performing 1D simulations using the symmetrically expanding cylindrical fusion plasma model. We discuss possible energy loss mechanisms, and account for these effects in our model by considering the corresponding temperature drop, $kT(t)$, of the fusion plasma as it expands in time sweeping the cold background gas jet region. Despite the nonlinear dependence of the neutron yield on laser cluster parameters, our study shows that we can expect a scaling law that is nearly linear above ~ 10 keV. During our analysis, we calculated the expected neutron yield as a function of the laser pulse energy, ion temperature, and ion number density using the cylindrical fusion plasma model. Our calculations revealed an excellent agreement with the available neutron yield data. For the first time, we calculated the expected scaling exponent for the temperature range of 1–100 keV and analyzed the observed temperature dependence of β by examining the temperature dependence of the Beam–Beam (BB) and Beam–Target (BT) fusion neutron yields separately.

2. Calculation of neutron yield

In laser-cluster fusion experiments, deuterium clusters are often used as the fuel to drive DD nuclear fusion reactions [5, 10, 12, 23, 24, 28–31]. A cluster is the intermediate state of matter between a single molecule and a bulk solid [5], which is an aggregate of many atoms or molecules combined together via van der Waals forces [32]. Deuterium clusters are produced when cryogenically cooled (80 – 100 K) deuterium gas under a high backing pressure (~ 50 bar) passes through a supersonic nozzle and expands into vacuum [33]. When irradiated with an ultra-intense laser pulse, deuterium clusters absorb a significant portion ($>90\%$) of the incident laser pulse energy [3], and high-temperature deuterium fusion plasmas (~ 10 keV) are generated [5].

Figure 1(a) illustrates a symmetrically expanding cylindrical fusion plasma. After the deuterium gas exits the supersonic nozzle, an intense laser pulse is focused on the deuterium cluster jet. Deuterium clusters are instantly ionized by the strong laser field [34], and energetic deuterium ions are produced after the clusters undergo Coulomb explosion [35]. The resulting fusion plasma is formed with an approximately cylindrical shape because the incident laser beam typically has a round focus and a long Rayleigh length, comparable to the nozzle diameter [11]. In figure 1(a), the initial plasma radius (r_0) becomes $r(t) = r_0 + \int_0^t v_{\text{avg}}(t') dt'$ after time t ,

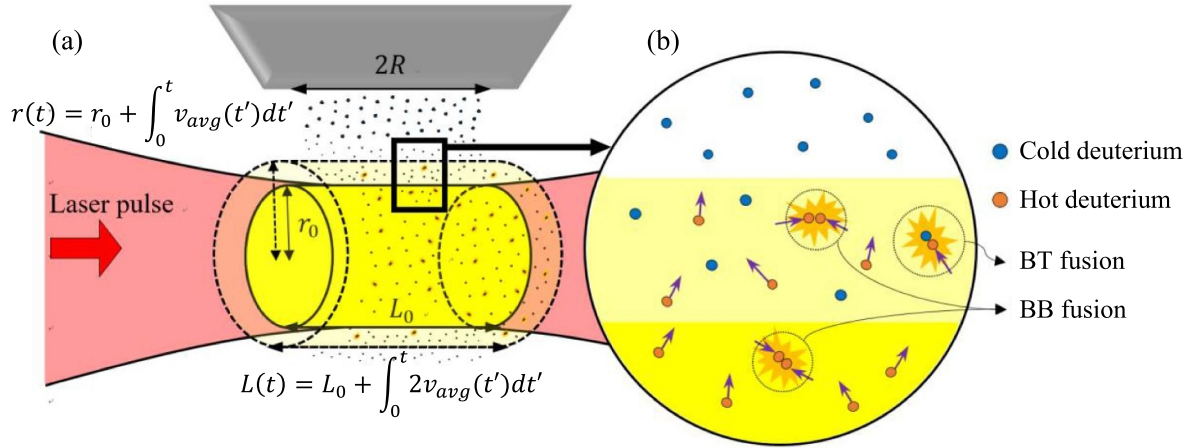


Figure 1. (a) Cylindrical fusion plasma model. An intense laser pulse irradiates the clusters and produces a cylindrical fusion plasma. The initial plasma with a radius of r_0 and a length of L_0 expands to $r(t)$ and $L(t)$ at an average ion speed of $v_{avg}(t')$. (b) Illustration showing the beam–beam (BB) and beam–target (BT) nuclear fusion reaction. (yellow area), BB fusion reactions can happen when two energetic deuterium ions collide with each other. As the fusion plasma expands over time (light yellow area), BT fusion reactions can also occur when hot deuterium ions collide with cold deuterium atoms or ions in the background gas jet.

where $v_{avg}(t')$ is the average speed of energetic deuterium ions. Likewise, the initial plasma length (L_0) becomes $L(t) = L_0 + \int_0^t 2v_{avg}(t') dt'$ after time t . In our model, L_0 is approximated as the diameter ($=2R = 5$ mm) of the nozzle opening [5]. (See supplementary figure S7 for simulation results using different L_0).

Nuclear fusion reactions can occur when energetic deuterium ions from different clusters collide with each other within the plasma or when they collide with the cold deuterium atoms or ions in the background gas [36]. The former reaction accounts for the BB fusion reaction, and the latter accounts for the BT fusion reaction [17, 36]. Figure 1(b) depicts the nuclear fusion reactions corresponding to the BB and BT fusion reactions. The initial fusion plasma (yellow area) consists of energetic deuterium ions, and the fusion reactions primarily occur owing to BB interactions. As the plasma expands (light-yellow area) in time, energetic deuterium ions collide with cold deuterium atoms or ions outside the hot plasma, and the BT fusion reactions can also occur along with the BB reactions.

The total fusion neutron yield (Y) is given as the sum of the BB (Y_{BB}) and BT (Y_{BT}) fusion yields [23]:

$$\begin{aligned}
 Y &= Y_{BB} + Y_{BT} \\
 Y_{BB} &= \int \frac{1}{2} n_d(t)^2 f(\vec{v}_1) f(\vec{v}_2) \sigma(v) v d\vec{v}_1 d\vec{v}_2 dV dt \\
 &= \frac{1}{2} N_{ion}^2 \int_0^\infty \langle \sigma v \rangle_{kT(t)} \frac{1}{V(t)} dt
 \end{aligned} \quad (1)$$

$$\begin{aligned}
 Y_{BT} &= N_{ion} \int n_d f(\vec{v}_1) \sigma(v_1) d\vec{v}_1 d\vec{l} \\
 &= N_{ion} n_d \int_0^\infty \langle \sigma \rangle_{kT(t)} v_{avg}(t) \frac{V_{cold}(t)}{V(t)} dt
 \end{aligned} \quad (2)$$

where $n_d(t)$ is the number density of energetic deuterium ions at time t , $f(\vec{v})$ is the velocity distribution function of deuterium ions, \vec{v}_1 and \vec{v}_2 are the velocities of the colliding deuterium ions, v is the relative speed, $\sigma(v)$ is the DD fusion cross section [2], N_{ion} is the total number of deuterium ions within the plasma, $\langle \sigma v \rangle_{kT(t)} = \int f(\vec{v}_1) f(\vec{v}_2) \sigma(v) v d\vec{v}_1 d\vec{v}_2$ is the DD fusion reactivity at an ion temperature of $kT(t)$, $\langle \sigma \rangle_{kT(t)} = \int f(\vec{v}_1) \sigma(v_1) d\vec{v}_1$ is the average cross section for BT fusion reactions at ion temperature $kT(t)$, $n_d (=n_d(t=0))$ is the atomic number density of deuterium, $V(t) = \pi r(t)^2 L(t)$ is the volume of the expanding cylindrical plasma at time t , and $V_{cold}(t)$ represents the volume of the plasma occupying the cold background gas jet region.

In our simulations, we have used $n_d(t) = N_{ion}/V(t)$, where N_{ion} is calculated from the energy conservation law $\eta E = \frac{3}{2} N_{ion} kT$ [17]. The ion energy conversion efficiency η represents the fractional laser pulse energy that went into the kinetic energy of the ions. While the conversion efficiency can depend on laser-cluster parameters such as the absorbed laser pulse energy, pulse duration, wavelength, and average size of the clusters, previous studies [21, 22] suggest a conversion efficiency of about 50% for an 800 nm laser pulse with a pulse duration below 100 fs. Therefore, we have used a conversion efficiency of 50% in our simulations. (See supplementary figure S8 for simulation results using different conversion efficiencies.) In addition, our simulations assume that the clusters within the cylindrical plasma are ionized completely, then the initial plasma volume V_0 is calculated from $V_0 = \pi r_0^2 L_0 = N_{ion}/n_d$ for each laser pulse energy. In summary, we can calculate Y_{BB} and Y_{BT} , knowing the incident laser pulse energy E , the initial number density of deuterium ions n_d , and the initial ion temperature $kT (=kT(t=0))$ of the fusion plasma using equations (1) and (2). Note that the ion temperature of the fusion plasma drops as the plasma expands in time. As the hot ions pass through the surrounding cold gas jet region, they undergo Coulomb collisions with the electrons

in the cold deuterium atoms in the gas medium. These interactions induce the energy transfer from the hot ions to the electrons via ionization and excitation processes, resulting in the energy loss of the hot ions. These energy losses can be estimated by calculating the stopping powers, and we have used a Monte Carlo simulation code, SRIM [37–39], for these calculations. (See supplementary figures S3–S6 for details.) The radiation loss from the fusion plasma seems negligible based on our estimates of the Bremsstrahlung radiation loss during the first 1 ns. For a 10 keV cylindrical plasma with an initial radius of 1 mm and a length of 5 mm at $n_d = 1.0 \times 10^{19} \text{ cm}^{-3}$, we estimate the radiation loss to be less than 0.001% of the total kinetic energy of the ions.

3. Linear scaling law of neutron yield for laser energy

In figure 2, the expected fusion neutron yields are shown as functions of the laser pulse energy from 0.1 J to 200 J using the cylindrical fusion plasma model. The hollow black triangles represent the expected neutron yield from a 10 keV fusion plasma with an atomic number density of $n_d = 10^{19} \text{ cm}^{-3}$, which predicts an almost linear fusion yield scaling law of $Y \propto E^{1.14}$. The hollow black circles also show the expected neutron yield from a 10 keV fusion plasma but with a lower number density of $n_d = 10^{18} \text{ cm}^{-3}$, which again suggests an approximately linear fusion yield scaling law of $Y \propto E^{1.14}$. We have also included the available neutron yield data in figure 2, and the experimental data are found to lie between the hollow black circles and the hollow black triangles. In figure 2, the maximum neutron yield from individual experiments is plotted as a black star [3], a green square [12], a red triangle [10], a red inverse triangle [24], a blue diamond [31], and blue circles [29]. A scaling exponent of 1.05 is obtained from the available neutron yield data [3, 10, 12, 24, 29, 31], which also suggests a nearly linear scaling law of the fusion neutron yield, $Y = 1.1 \times 10^5 E^{1.05}$.

In contrast, individual studies from previous experiments reported more favorable scaling exponents ranging from 1.6 to 2.3 [10, 12, 23, 24]. This discrepancy in the scaling law appears to result from various nonlinear effects of neutron yields for each experiment. In [12], the authors reported a scaling law of $Y \propto E^{2.2}$ in the laser energy range of 0.025 J to 0.12 J, where the authors claimed that the laser propagation effect on the gas plume caused a rapid increase in the neutron yield [12]. In [10, 23], the authors reported a scaling law of $Y \propto E^{1.6}$ in the range of 0.1–5.5 J. The authors found that the number of energetic ions increased linearly with laser energy and explained that the variation in the ion temperature with laser energy produced the observed scaling law [10]. In [24], the authors presented quadratic scaling exponents of 2.15 and 2.3, where the authors argued that focal geometries and pulse durations caused differences in the scaling laws [24].

The maximum neutron yield obtained from each experiment, however, shows an excellent agreement with the fusion neutron yield calculated using the cylindrical fusion plasma model. For example, [3, 4] reported 10^4 neutrons at 0.12 J with

an ion temperature of 5 keV. This observation agrees well with our neutron yield of 1.1×10^4 calculated using their experimental conditions. In [12], the authors reported a maximum neutron yield of 1.2×10^4 neutrons per shot with a 0.12 J laser pulse for $n_d = 1.5\text{--}2.0 \times 10^{19} \text{ cm}^{-3}$. This observation also agrees well with our calculated neutron yield of 1.0×10^4 neutrons per shot using $n_d = 1.75 \times 10^{19} \text{ cm}^{-3}$. Reference [23] reported a maximum neutron yield of 6.0×10^5 neutrons per shot at 5.5 J, and [24] reported 2.0×10^6 neutrons per shot at 9.7 J. Using the experimental conditions in [23, 24], we expect fusion neutron yields of 6.9×10^5 neutrons per shot at 5.5 J and 1.6×10^6 neutrons per shot at 9.7 J. In [29], the authors reported maximum neutron yields of 7.2×10^6 at 52 J and 1.6×10^7 at 102 J using plasma mirrors. In [5], the authors reported 1.9×10^7 at 172 J. Again, these yield measurements are consistent with our calculated neutron yields of 5.8×10^6 at 52 J, 1.2×10^7 at 102 J, and 1.9×10^7 at 172 J when using their experimental conditions in our model.

4. Dependence of neutron yield on E and kT

The dependence of the calculated neutron yield on E and kT is examined in figure 3. The hollow black circles, hollow blue triangles, and hollow red squares represent the calculated neutron yield as a function of kT at 1 J, 10 J, and 100 J, respectively, with $n_d = 10^{19} \text{ cm}^{-3}$. The DD fusion reactivity (solid-green line) is also shown in figure 3 as a reference. In figure 3, the DD fusion reactivity increases by more than six thousand times in the range of 1–10 keV, while neutron production increases by 613 times at 1 J, 345 times at 10 J, and 257 times at 100 J. In the range of 10–100 keV, the DD fusion reactivity increases by approximately 45 times, while the neutron yield increases by approximately 10 times or less. Although both the neutron yield and DD fusion reactivity increase with the ion temperature, the increase in the fusion neutron yield is much slower than that in the DD fusion reactivity.

The observed trend in figure 3 can be understood as a consequence of N_{ion} being inversely proportional to kT in our model. An increase in the fusion reactivity does not directly translate to an increase in the fusion yield because a higher ion temperature implies fewer energetic ions for a given laser pulse energy. The moderate increase in the fusion neutron yield predicted in figure 3 is also consistent with laser-cluster fusion experiments using CD_4 clusters as the target [23, 36]. In those experiments, CD_4 clusters were used, and higher ion temperatures were often achieved [40–42]. Interestingly, the reported fusion neutron yield is lackluster because of the much lower atomic number density in those experiments. For example, 7×10^3 neutrons were produced using a 0.8 J laser pulse with CD_4 clusters in [36]. Although the ion temperature was fairly high (~ 27 keV), the number density was very low ($\sim 2 \times 10^{17} \text{ cm}^{-3}$), and the resulting fusion yield was small.

The modest increase in the neutron yields at high ion temperatures can be understood better by examining the temperature dependence of the BB and BT yields separately. Figure 4 shows the calculated neutron yields from the BB (hollow

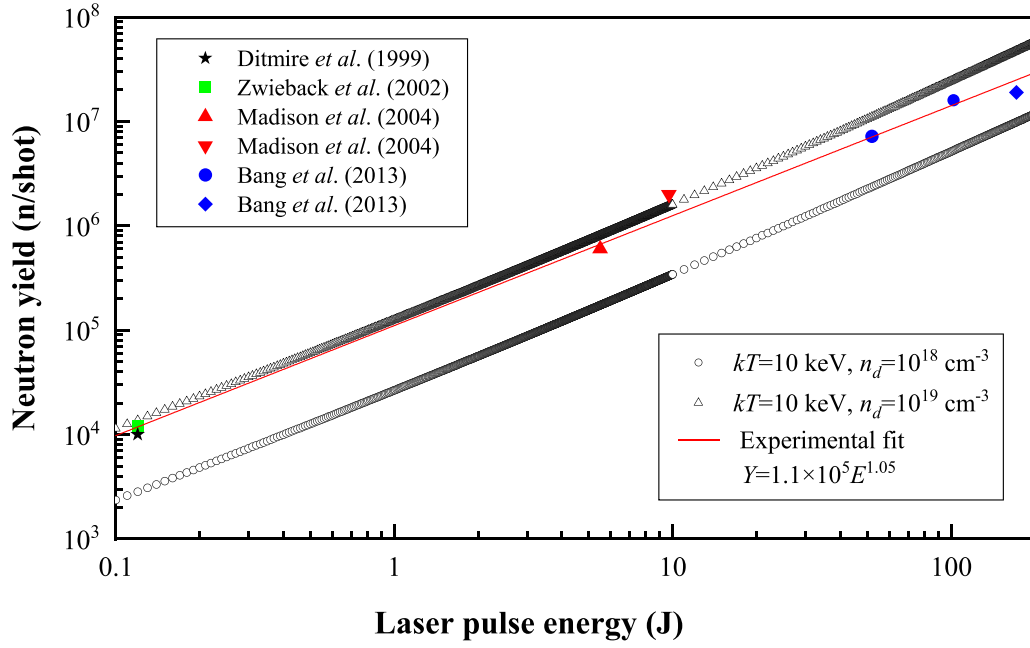


Figure 2. Fusion neutron yield is shown as a function of the input laser pulse energy. The hollow black circles represent the calculated neutron yields at 10 keV and $n_d = 10^{18} \text{ cm}^{-3}$, and the hollow black triangles indicate the calculated neutron yields at 10 keV and $n_d = 10^{19} \text{ cm}^{-3}$. The scaling law for the neutron yields reported from previous experiments is shown as a solid red line.

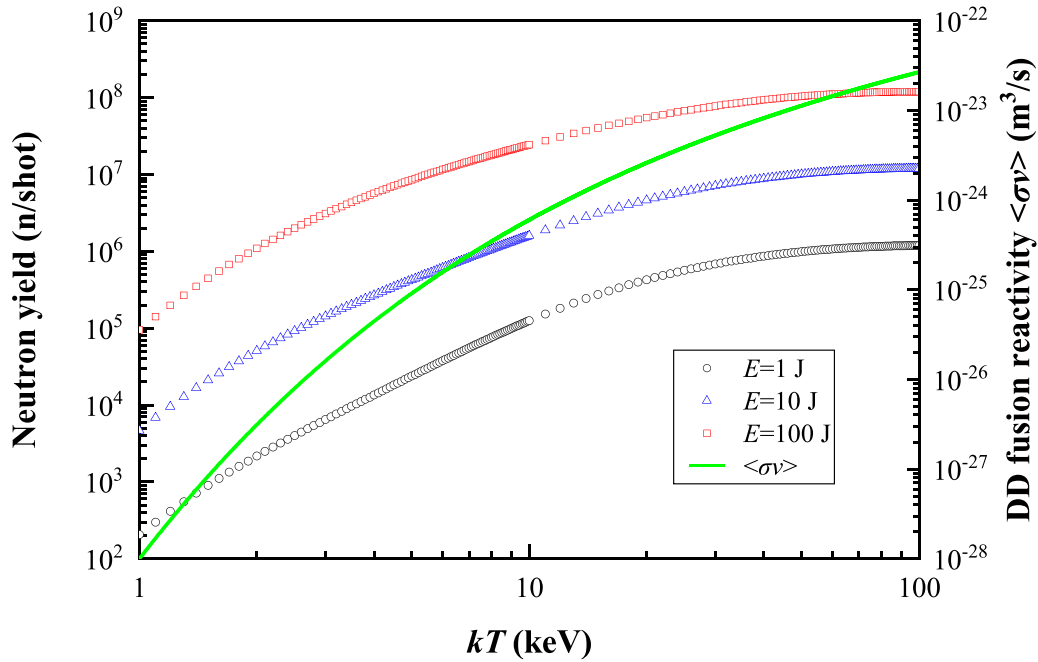


Figure 3. Calculated neutron yields are shown at three laser pulse energies as functions of deuterium ion temperature from 1 keV to 100 keV. Hollow black circles, hollow blue triangles, and hollow red squares show the neutron yield when the laser pulse energy is 1 J, 10 J, and 100 J, respectively. While the DD fusion reactivity increases rapidly in the 1–100 keV range, the neutron yields are found to increase only modestly with the deuterium ion temperature.

circles) and BT fusion reactions (hollow triangles) as functions of the deuterium ion temperature for the laser pulse energies of 1 J (blue) and 100 J (red). In both cases, the BB yields are dominant at low ion temperatures ($<4 \text{ keV}$ for 1 J and $<10 \text{ keV}$ for 100 J). Then, the BT yields become dominant as the ion temperature increases. As the ion temperature increases above

$\sim 10 \text{ keV}$, the BB yields increase marginally and then decrease after reaching maximum yields. In comparison, the BT yields continue to increase moderately above 10 keV. Therefore, the modest increase in the total neutron yields can be explained by the decrease in the BB yield and by the moderate increase in the BT yield above $\sim 10 \text{ keV}$.

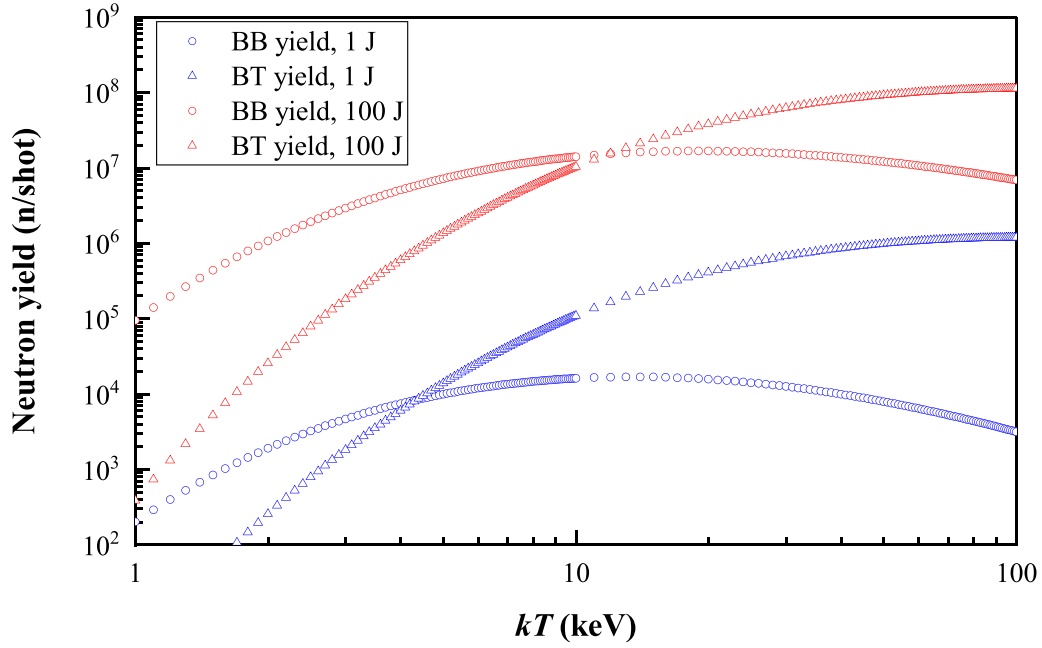


Figure 4. Neutron yields from BB (hollow circles) and BT fusion reactions (hollow triangles) are shown as functions of the deuterium ion temperature at laser pulse energies of 1 J (red) and 100 J (blue) for $n_d = 10^{19} \text{ cm}^{-3}$.

In figures 3 and 4, the neutron yield curves have similar shapes for different laser pulse energies. The increasing trend of the BB and BT yields is explained by approximate equations for ion temperature. According to equations (1) and (2), the BB and BT yields are proportional to N_{ion}^2 and N_{ion} , respectively. Using the energy conservation law $\eta E = \frac{3}{2} N_{\text{ion}} kT$, the BB and BT yields can now be written as $\sim \frac{\langle \sigma v \rangle_{kT}}{kT^2}$ and $\sim \frac{\langle \sigma \rangle_{kT}}{kT}$, respectively. When we calculate $\langle \sigma v \rangle_{kT}$ and $\langle \sigma \rangle_{kT}$, the latter increases seven times faster than the former in the energy range from 1 keV to 100 keV. This rate results in a much faster increase in the BT yield than that in the BB yield. Our calculations indicate that the total fusion neutron yield is dominated by the BT yield for ion temperatures above 10 keV.

5. Dependence of scaling laws on kT

Our scaling law shows that the neutron yield increases nearly linearly with laser pulse energy at high ion temperatures above 10 keV. We calculated the neutron yield scaling law $Y = \alpha E^\beta$ for laser pulse energies from 0.1 J to 200 J varying the initial ion temperature and ion number density. Figure 5 shows the temperature dependence of β at two gas densities. Each data point in figure 5 represents the scaling exponent extracted from a plot of fusion yield versus laser energy for a given initial ion temperature and ion number density. (See supplementary figure S1) The hollow blue circles and hollow red triangles represent the scaling exponents for $n_d = 10^{18} \text{ cm}^{-3}$ and $n_d = 10^{19} \text{ cm}^{-3}$, respectively, in the 1–100 keV range. As the ion temperature increases, the scaling exponents decrease quickly and approach 1.0 in both cases. In figure 5, the scaling exponent seems to present a weak dependence on the ion number density at temperatures above 10 keV. For example,

the scaling exponent is 1.14 for both $n_d = 10^{18} \text{ cm}^{-3}$ and $n_d = 10^{19} \text{ cm}^{-3}$ at 10 keV.

We assumed that the scaling law of the total fusion yields consists of the scaling laws of the BB and BT yields,

$$Y = Y_{\text{BB}} + Y_{\text{BT}} \\ \alpha E^\beta = \alpha_{\text{BB}} E^{\beta_{\text{BB}}} + \alpha_{\text{BT}} E^{\beta_{\text{BT}}}, \quad (3)$$

where α_{BB} , α_{BT} , and α are the scaling constants of the BB, BT, and total yields, respectively, and β_{BB} , β_{BT} , and β are their respective exponents.

Figure 6 shows β (red circles), β_{BB} (hollow red triangles), β_{BT} (hollow red squares), and $\alpha_{\text{BT}}/\alpha_{\text{BB}}$ (hollow blue diamonds) as functions of the ion temperature when the ion density is fixed at 10^{19} cm^{-3} . $\alpha_{\text{BT}}/\alpha_{\text{BB}}$ is the ratio of the BT and BB yield coefficients in equation (3). β is initially dominated by β_{BB} because $\alpha_{\text{BT}}/\alpha_{\text{BB}}$ is small at low temperatures. As the ion temperature increases, β approaches β_{BT} because $\alpha_{\text{BT}}/\alpha_{\text{BB}}$ increases. The rapid decrease of β with ion temperature is related to the modest increase in the neutron yield above ~ 10 keV as discussed in section 4. In fact, β_{BB} and β_{BT} can be treated as ~ 1.6 and 1.0 , respectively, because they rarely change with ion temperature at temperatures above ~ 10 keV. For ion temperatures above 10 keV, figure 6 shows that β becomes less than 1.14, resulting in a nearly linear scaling law for high temperature fusion plasmas above 10 keV.

The scaling exponents shown in figures 5 and 6 are somewhat different from those found in previous theoretical studies. In [12], the authors suggested a scaling exponent of 1.5 based on a crude fusion yield model accounting for the BB fusion reaction only. In [11], a scaling exponent of 1.2 was obtained from a slightly more sophisticated model that accounted for

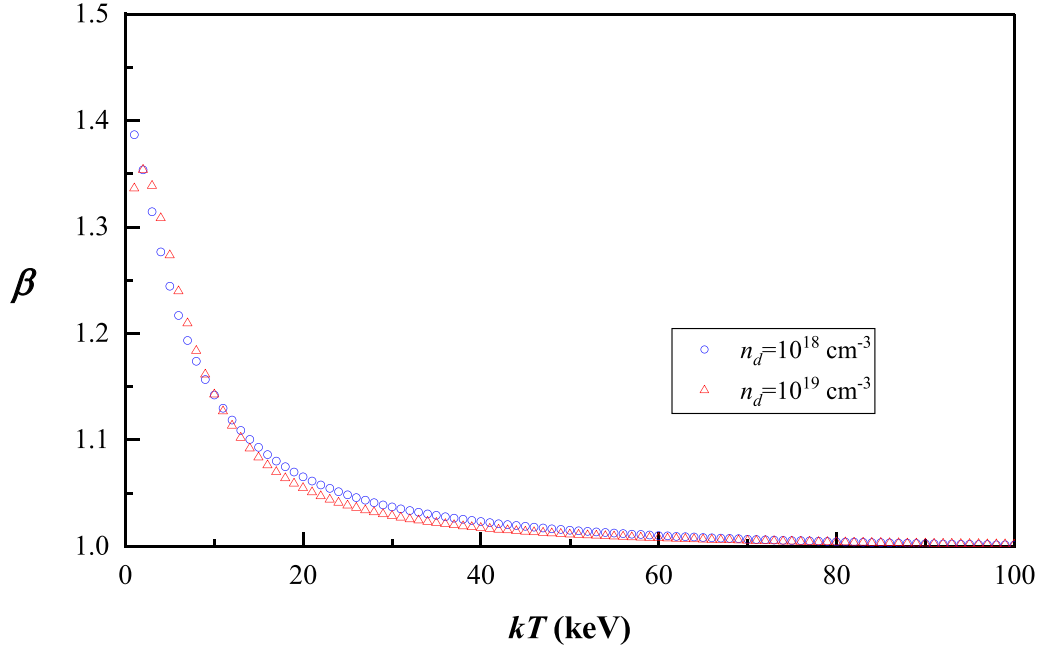


Figure 5. Exponents (β) of the scaling laws ($Y = \alpha E^\beta$) are shown as functions of deuterium ion temperatures from 1 keV to 100 keV in 1 keV steps at two different ion number densities of $n_d = 1.0 \times 10^{18} \text{ cm}^{-3}$ (hollow blue circles) and $n_d = 1.0 \times 10^{19} \text{ cm}^{-3}$ (hollow red triangles). For each ion temperature and gas density, the corresponding scaling exponent, β , was obtained from the calculated fusion yields for laser energies varying from 0.1 J to 200 J.

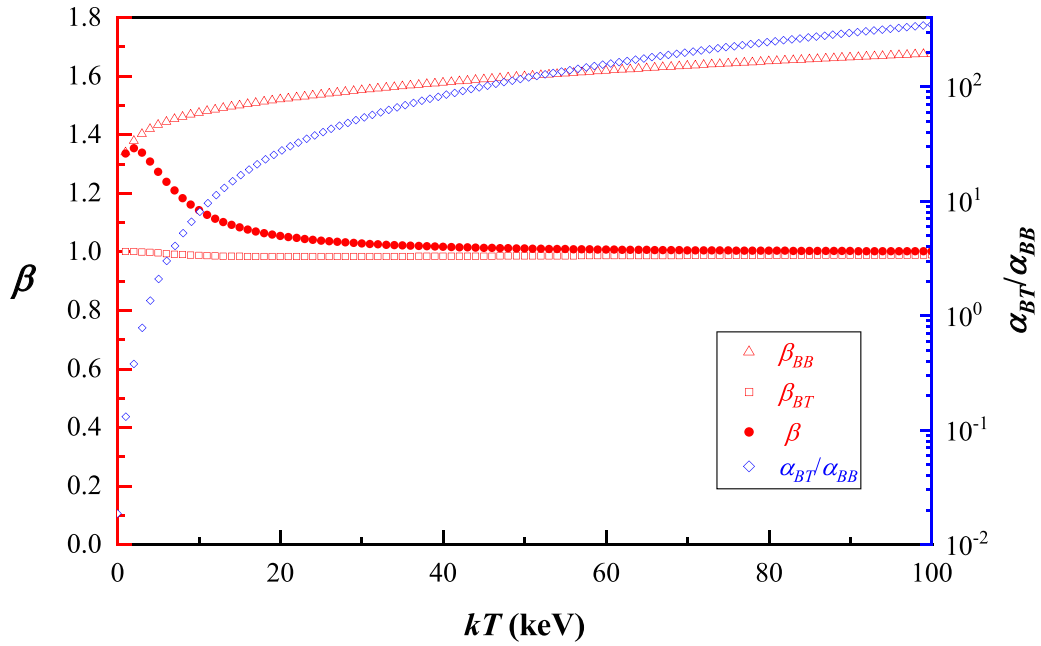


Figure 6. Scaling exponents (β , β_{BB} , β_{BT}) and the ratio of coefficients (α_{BT}/α_{BB}) are shown as functions of the ion temperature. The scaling law for the total neutron yield is expressed as the sum of the scaling laws of the BB and BT yields ($\alpha E^\beta = \alpha_{BB} E^{\beta_{BB}} + \alpha_{BT} E^{\beta_{BT}}$).

the attenuation of laser pulse energy and the known cluster size distribution. This scaling exponent is quite close to ours, but their model neglects the temperature dependence of the scaling exponent.

In our simulations, we have used a cylindrical plasma of 5 mm length to calculate the fusion neutron yields. Since the calculated neutron yield depends on the geometry of the fusion

plasma, we have investigated fusion plasmas with slightly different geometries. For example, we have examined the robustness of our conclusions by performing similar simulations, varying the plasma lengths. (See supplementary figure S7 to see the scaling exponents (β) as functions of kT for different plasma lengths.) Again, these additional simulation results show that the scaling exponent approaches 1.0

at higher ion temperatures above 10 keV for all plasma lengths.

While laser-cluster parameters are known to be correlated for the fusion neutron yields, our simulation results indicate that the fusion neutron yield will increase almost linearly with the laser pulse energy for high temperature fusion plasmas above 10 keV. In laser-cluster fusion experiments, parameters that affect the ion temperature, such as average size and spatial distribution of clusters, pulse duration, and spot size, can be optimized independently of the laser pulse energy and ion density for a maximum fusion yield. Our findings will provide theoretical support for establishing an experimental scheme for maximum fusion neutron yields.

6. Conclusion

Using the cylindrical fusion plasma model, we calculated the expected neutron yields from laser-cluster fusion experiments as a function of the laser pulse energy, ion temperature, and ion number density. While certain earlier studies have reported more favorable scaling exponents in the range of 1.6–2.3 based on their own experimental findings, our simulation results suggest a scaling law of $Y \sim E^{1-1.35}$ for the fusion neutron yields with laser pulse energy in the 0.1–200 J regime. In particular, our simulations show that the scaling exponent approaches 1.0 for high-temperature fusion plasmas above 10 keV. Even with the strong nonlinear dependence of the DD fusion reactivity on the ion temperature, our study indicates that we can expect a neutron yield scaling law that is almost linear above 10 keV, and the number of fusion neutrons per joule of incident laser energy does not increase significantly with laser energy.

By independently analyzing the temperature dependences of the BB and BT fusion yields, we attempted to explain the observed temperature dependence of the scaling exponent. While our fusion neutron yield scaling law differs from previously reported scaling laws obtained from individual experiments, it is in excellent agreement with the scaling law determined by each experiment's maximum neutron yield. We anticipate that our scaling law will serve as a valuable guide for future laser-cluster fusion experiments in the high laser energy regime above ~ 1 kJ, providing correct estimates of the maximum achievable fusion yields at high laser energies.

Acknowledgments

This work was supported by the National Research Foundation of Korea (NRF) grant funded by the Korea government (MSIT) (No. 2023R1A2C1002912) and by the Institute for Basic Science under IBS-R012-D1.

ORCID iDs

Junho Won  <https://orcid.org/0000-0001-9481-394X>
 Woosuk Bang  <https://orcid.org/0000-0002-4259-1342>

References

- [1] Balantekin A.B. and Takigawa N. 1998 *Rev. Mod. Phys.* **70** 77–100
- [2] Bosch H.-S. and Hale G.M. 1992 *Nucl. Fusion* **32** 611
- [3] Ditmire T., Zweiback J., Yanovsky V.P., Cowan T.E., Hays G. and Wharton K.B. 1999 *Nature* **398** 489
- [4] Ditmire T., Zweiback J., Yanovsky V.P., Cowan T.E., Hays G. and Wharton K.B. 2000 *Phys. Plasmas* **7** 1993
- [5] Bang W. et al 2013 *Phys. Rev. Lett.* **111** 055002
- [6] Barbui M. et al 2013 *Phys. Rev. Lett.* **111** 082502
- [7] Lattuada D. et al 2016 *Phys. Rev. C* **93** 045808
- [8] Barbarino M. et al 2016 *Int. J. Mod. Phys. E* **25** 1650063
- [9] Alvarez J., Fernández-Tobías J., Mima K., Nakai S., Kar S., Kato Y. and Perlado J.M. 2014 *Phys. Proc.* **60** 29
- [10] Madison K.W., Patel P.K., Allen M., Price D., Fitzpatrick R. and Ditmire T. 2004 *Phys. Rev. A* **70** 053201
- [11] Li H., Liu J., Ni G., Li R. and Xu Z. 2009 *Phys. Rev. A* **79** 043204
- [12] Zweiback J., Cowan T.E., Hartley J.H., Howell R., Wharton K.B., Crane J.K., Yanovsky V.P., Hays G., Smith R.A. and Ditmire T. 2002 *Phys. Plasmas* **9** 3108
- [13] Fennel T., Meiwe-Broer K.H., Tiggesbäumker J., Reinhard P.G., Dinh P.M. and Suraud E. 2010 *Rev. Mod. Phys.* **82** 1793
- [14] Breizman B.N., Arefiev A.V. and Fomyts'kyi M.V. 2005 *Phys. Plasmas* **12** 056706
- [15] Kundu M. and Bauer D. 2006 *Phys. Rev. Lett.* **96** 123401
- [16] Lu H.Y. et al 2009 *Phys. Rev. A* **80** 051201
- [17] Bang W. 2015 *Phys. Rev. E* **92** 013102
- [18] Last I. and Jortner J. 2004 *J. Chem. Phys.* **121** 3030
- [19] Petrov G.M., Davis J., Velikovich A.L., Kepple P., Dasgupta A. and Clark R.W. 2005 *Phys. Plasmas* **12** 063103
- [20] Holkundkar A.R., Mishra G. and Gupta N.K. 2014 *Phys. Plasmas* **21** 013101
- [21] Davis J., Petrov G.M. and Velikovich A.L. 2006 *Phys. Plasmas* **13** 064501
- [22] Petrov G.M., Davis J. and Velikovich A.L. 2006 *Plasma Phys. Control. Fusion* **48** 1721
- [23] Madison K.W., Patel P.K., Price D., Edens A., Allen M., Cowan T.E., Zweiback J. and Ditmire T. 2003 *Phys. Plasmas* **11** 270
- [24] Madison K.W., Patel P.K., Allen M., Price D. and Ditmire T. 2003 *J. Opt. Soc. Am. B* **20** 113
- [25] Krása J. and Klír D. 2020 *Front. Phys.* **8** 310
- [26] Sakabe S., Hashida M., Tokita S. and Otani K. 2009 *Plasma Fusion Res.* **4** 041
- [27] Kimura S. and Bonasera A. 2013 *Int. J. Mod. Phys. E* **21** 12
- [28] Zweiback J., Cowan T.E., Smith R.A., Hartley J.H., Howell R., Steinke C.A., Hays G., Wharton K.B., Crane J.K. and Ditmire T. 2000 *Phys. Rev. Lett.* **85** 3640
- [29] Bang W., Dyer G., Quevedo H.J., Bernstein A.C., Gaul E., Rougk J., Aymond F., Donovan M.E. and Ditmire T. 2013 *Phys. Plasmas* **20** 093104
- [30] Bang W., Dyer G., Quevedo H.J., Bernstein A.C., Gaul E., Donovan M. and Ditmire T. 2013 *Phys. Rev. E* **87** 023106
- [31] Bang W. et al 2013 *Phys. Rev. E* **88** 033108
- [32] Castleman A.W. and Keesee R.G. 1988 *Science* **241** 36–42
- [33] Bang W. et al 2014 *Phys. Rev. E* **90** 063109
- [34] Zweiback J., Smith R.A., Cowan T.E., Hays G., Wharton K.B., Yanovsky V.P. and Ditmire T. 2000 *Phys. Rev. Lett.* **84** 2634
- [35] Ditmire T., Donnelly T., Rubenchik A.M., Falcone R.W. and Perry M.D. 1996 *Phys. Rev. A* **53** 3379

- [36] Grillon G. *et al* 2002 *Phys. Rev. Lett.* **89** 065005
- [37] Song C., Won J., Song J. and Bang W. 2022 *Int. Commun. Heat Mass Transfer* **135** 106070
- [38] Song C., Lee S. and Bang W. 2022 *Sci. Rep.* **12** 15173
- [39] Ziegler J.F., Ziegler M.D. and Biersack J.P. 2010 *Nucl. Instrum. Methods Phys. Res. B* **268** 1818
- [40] Song J., Won J., Bang W. and Wu X. 2021 *PLoS One* **16** e0261574
- [41] Zhang H., Lu H., Li S., Xu Y., Guo X., Leng Y., Liu J., Shen B., Li R. and Xu Z. 2014 *Appl. Phys. Express* **7** 026401
- [42] Li S. *et al* 2013 *Phys. Plasmas* **20** 043109